



# In-Silico Screening the Nitrogen Reduction Reaction on Single-Atom Electrocatalysts Anchored on MoS<sub>2</sub>

Liang Xu<sup>1</sup> · Miao Xie<sup>1</sup> · Hao Yang<sup>1</sup> · Peiping Yu<sup>1</sup> · Bingyun Ma<sup>1</sup> · Tao Cheng<sup>1</sup> · William A. Goddard III<sup>2</sup>

Accepted: 25 November 2021 / Published online: 8 January 2022

© The Author(s), under exclusive licence to Springer Science+Business Media, LLC, part of Springer Nature 2021

## Abstract

We show that a Single-Atom Electrocatalyst (SAC) for the Nitrogen Reduction Reaction (NRR) can provide an environmentally green alternative to the Haber–Bosch high-temperature high-pressure process, replacing the water gas shift production of H<sub>2</sub> with H extracted from water. Anchoring the single atom on a two-dimensional substrate provides control to tune NRR catalytic performance toward a SAC possessing high utilization, high activity, and high selectivity. Experimental results suggest that this can significantly improve the activity and selectivity of NRR, but the specific reaction mechanism remains uncertain. This makes it difficult to select new catalytic materials for further optimization. Here we use Density Functional Theory to study the NRR catalytic mechanism on a catalytic model using a MoS<sub>2</sub> substrate to support a single atom site. We correct for solvation effects on the electrochemical reactions. We started with Fe@MoS<sub>2</sub>, for which there are promising experimental reports, and conducted a systematic study of the NRR reaction mechanisms. These results show that N<sub>2</sub> adsorption, hydrogenation of N<sub>2</sub>, desorption of NH<sub>3</sub>, and Hydrogen Evolution are all critical steps affecting the reaction rates. Based on these steps, we scanned 23 transition metal elements to find improved catalysts. We identified Ir@MoS<sub>2</sub> (Mo top site) as the best candidate, predicted to have good catalytic activity and selectivity with 64.11% Faraday Efficiency. These results on the mechanism for NRR and the in silico search for alternative catalysts provide new promising targets for synthesizing novel and efficient SAC@MoS<sub>2</sub> NRR catalysts.

**Keywords** Density Functional Theory · Implicit solvation · Electrochemical catalysis · Rational catalysis design · Computational modeling

## 1 Introduction

Humanity is facing multiple threats in energy resources while confronting global warming and environmental deterioration. It is urgent to change the current energy structure to promote a sustainable production model. One of the key targets is the reduction of N<sub>2</sub> to ammonia (NH<sub>3</sub>) used in manufacturing the synthetic chemical fertilizer needed to sustain the growing population and also for green fuels and explosives [1–3].

✉ Tao Cheng  
tcheng@suda.edu.cn

✉ William A. Goddard III  
wag@caltech.edu

<sup>1</sup> Institute of Functional Nano and Soft Materials (FUNSOM), Soochow University, Suzhou 215123, China

<sup>2</sup> Materials and Process Simulation Center, California Institute of Technology, Pasadena, CA 91125, USA

However, almost all synthetic NH<sub>3</sub> is now produced via the Haber–Bosch process, which requires severe conditions of 400–500 °C and 150–250 atm, accounting for 1–2% of the global energy consumption. Moreover, producing the H<sub>2</sub> needed via water gas shift (CO + H<sub>2</sub>O → CO<sub>2</sub> + H<sub>2</sub>) releases 1.5 tons CO<sub>2</sub> per ton of NH<sub>3</sub>, contributing ~1.4% of anthropogenic CO<sub>2</sub> emissions to global warming [4]. Thus, it is essential we need to improve the industrial synthetic methodology to realize NRR under ambient temperature and atmospheric pressure [5, 6].

We focus here on electrochemical synthesis since it eliminates the environmentally costly need for H<sub>2</sub>, obtaining the required hydrogen atoms from water, and it can operate at room temperature and atmospheric pressure. This has advantages of high efficiency, zero-emission, low energy consumption, without CO<sub>2</sub> production. However, the N<sub>2</sub> reduction rate depends sensitively on catalytic activity and selectivity, requiring the discovery of new high-performance catalysts. Thus our focus is to rationally discover

new candidate electrochemical catalysts for N<sub>2</sub> reduction to NH<sub>3</sub>. The development of high-performance electrocatalysts faces significant challenges, with tremendous obstacles concerning catalyst structural stability, absorption of N<sub>2</sub>, hydrogenation of N<sub>2</sub>, desorption of NH<sub>3</sub>, and competition with the Hydrogen Reduction Reaction (HER).

For metal catalysts, Goddard and coworkers [7] compared the mechanism and reaction kinetics for both thermal and electrochemical NRR (Nitrogen Reduction Reaction) on Ru(0001), showing that electrochemical reactions can lead to a low barrier for the Potential Determined Step (PDS) compared to the thermal catalytic reaction.

The major NRR catalysts can be partitioned into:

- metals (Au, Ru, Mo) [8–12], but these noble metals and intermetallic compounds present problems with stability, high cost, scarcity, and low selectivity.
- sulfides (MoS<sub>2</sub>, WS<sub>2</sub>) [6, 13], where Sun et al. [6] studied MoS<sub>2</sub> as a catalyst for NRR and discovered that MoS<sub>2</sub> has highly efficient catalytic activity for the edge site but not for the basal plane
- nitrides (VN, ZrN, CrN and WN) [14, 15], where Skúlason et al. [12] studied 23 transition metal nitrides that catalyze NRR using theory, showing that RuN, CrN, and WN are stable and active for NRR with low onset potentials from –0.23 to –0.55 V versus reversible hydrogen electrode (RHE) among all the nitrides.
- carbides (Mo<sub>2</sub>C) [16], where Mukundan and coworkers [14] reported an origami-like Mo<sub>2</sub>C cathode catalyst for NRR that achieved a maximum synthesis rate of  $2.16 \times 10^{-11} \text{ mol cm}^{-2} \text{ s}^{-1}$  and a Faradaic Efficiency (FE) of 1.8%. Indeed, these origami-like structures contributed to improving electrochemical catalytic activity.
- oxides (Fe<sub>2</sub>O<sub>3</sub>, NbO<sub>2</sub>) [17, 18], where Gengfeng Zheng et al. [15] demonstrated that the NbO<sub>2</sub> nanoparticles have an outstanding ammonia production rate of  $11.6 \mu\text{g h}^{-1} \text{ mg cat}^{-1}$  at –0.65 V versus RHE and excellent electrochemical stability compared with Nb<sub>2</sub>O<sub>5</sub>.

The above catalysts exhibit promising catalytic activity, but all have problems that hamper large-scale applications. Thus, we want to discover new electrochemical catalysts that avoid the above shortcomings.

Recently, single-atom catalysts (SAC) have generated excitement because they can exhibit excellent physicochemical properties, such as strong metal-substrate interactions, unique coordination environments, and quantum size effects. These characteristics arise from the unique electronic structure of the active sites for SACs, which can be quite different from nano- and sub-nano clusters, leading to unique catalytic activity. Therefore, we consider that SAC's provide a promising strategy for NRR. Indeed progress has already been made:

- a LiN/Ni catalyst was synthesized experimentally for NRR to synthesize ammonia [19], showing catalytic activity comparable to that of Ru. Also, LiN/Ni is structurally stable and leads to a yield of  $5.5 \text{ mmol g}^{-1} \text{ h}^{-1}$  synthetic ammonia. The novel inspiration of LiN/Ni is the dual catalytic site that dramatically improves selectivity and catalyst utilization.
- Fe/N<sub>4</sub> has been synthesized on graphite, leading to a yield for ammonia formation of  $62.9 \mu\text{g h}^{-1} \text{ mg cat}^{-1}$ , with a Faraday efficiency of 18.6% [20].
- Qiao et al. [21] studied cost-effective carbon-based catalysts. They discovered that the catalytic activity of heterogeneous atoms (Se, Te) doped on a carbon-based catalyst leads to a performance superior to most metal catalysts on NRR.
- Feng et al. [22] studied MoS<sub>2</sub>-based doped single metal atom catalyst for NRR, discovering that the optimal MoS<sub>2</sub>-based doped atom is Re (onset potential 0.42 V).

Therefore, many researchers have focused on simple composite catalysts, including highly stable substrates and catalytic active atoms or clusters. But the development of efficient single-atom catalysts has been prolonged because of the difficulty of single-atom catalyst synthesis.

To provide a basis for rapidly developing efficient single-atom catalysts, it is essential to obtain a thorough understanding of the mechanisms of single-atom catalysts for NRR. Inspired by the essential role of Mo and S in natural nitrogenase, we selected the basal plane of the two-dimensional material MoS<sub>2</sub> as the substrate to support the single transition metal atom in the composite SAC [23]. Although MoS<sub>2</sub> has been reported to exhibit activity towards HER, it is more likely, despite of the debates, that the catalysis activity comes from defects or edge, instead of basal plane. Instead, the basal plane MoS<sub>2</sub> can serve as a support for foreign metal to facilitate catalytic activity towards N<sub>2</sub>RR [24]. We examined the mechanism using DFT (Density Functional Theory) calculations, including an implicit solvation model [25]. We first studied the mechanisms of NRR on Fe@MoS<sub>2</sub> to verify the feasibility of SAC@MoS<sub>2</sub> applied to NRR, and then we screened the important intermediates for 23 possible SACs@MoS<sub>2</sub> to identify the best candidates. These comprehensive simulation results suggest Ir@MoS<sub>2</sub> (Mo top site) as the most promising SAC catalyst.

## 2 Models and Methods (Computational Details)

The calculations were performed using the spin-polarized DFT method as implemented in the Vienna ab initio simulation package (VASP 5.4.4) [26, 27]. The exchange–correlation (XC) function of the generalized gradient approximation

(GGA-PBE) was applied for describing the XC energy. The projector augmented wave (PAW) method was utilized for the treatment of electron–ion interactions [28–30]. Van der Waals (vdW) interactions were taken into account by using the PBE-D<sub>3</sub> method [31–34]. The implicit solvation model was used to mimic reaction conditions close to the actual experimental situation. [35].

The MoS<sub>2</sub> model was a 4×4×1 supercell. The Brillouin zone was sampled using a 3×3×1 grid for geometry optimization. The single metal atom was anchored either at the Mo top site or the hollow site of MoS<sub>2</sub>. We set a 20 Å vacuum layer along the z-axis to prevent interactions between adjacent periodic images. For the plane-wave (PW) basis, we selected a 400 eV cut-off, because benchmarks using a cut-off of 500 eV and 600 eV led to insignificant changes.

The atoms were relaxed until the maximum residual force and energy went below the threshold value of 0.01 eV Å<sup>-1</sup> and 10<sup>-6</sup> eV.

Complete mechanisms for NRR have been published previously, with 12 steps required for Haber Bosch [36] and a similar number for electrocatalytic NRR [37]. These studies involved very detailed examinations of the binding of intermediates and electrocatalytic NRR, including solvent H<sub>2</sub>O, OH, and H bound to the catalysts. In this paper, we simplify the calculations to do in silico optimization over many SACs.

To systematically evaluate stability and catalytic activity of the catalyst, we calculated the binding energies of SACs anchored on the surface of MoS<sub>2</sub>, the cohesive energies of the bulk transition metal, and the Gibbs free energy change for four critical elementary steps on the SAC@MoS<sub>2</sub>, including

- the adsorption of N<sub>2</sub>,
- the adsorption of H,
- the desorption of NH<sub>3</sub> and
- the formation energies of the first hydrogenated \*N<sub>2</sub> (\* absorbed state).

Here we used the simple Computational Hydrogen Electrode (CHE), proposed by Norskov et al. [38]

$$G_{298.15} = E^{\text{sol}} + E_{\text{zpe}} + H(298) - TS \quad (1)$$

where E is the DFT energy of intermediates in each elementary step during NRR, E<sup>sol</sup> includes the implicit solvation correction to E, E<sub>zpe</sub> is the zero point vibration energy correction to E, H(298) is the change in enthalpy from 0 to 298 K, and S is the adsorption entropy. The latter three are obtained through calculating the phonon frequencies, but only for the surface adsorbate [39].

Since we expect that the absorption entropy S of the intermediates (\*N<sub>2</sub>, \*N<sub>2</sub>H, \*NH<sub>3</sub>, \*H) on SAC@MoS<sub>2</sub> depends

little on the substrate, we replaced the absorption entropy S of the various intermediates on SAC@MoS<sub>2</sub> with the values calculated for the intermediate on Fe@MoS<sub>2</sub> (see Table S1). For structural stability, Hensen et al. mapped a scaling law from thermodynamics to kinetics using machine-learning methods. They reported that the diffusion barrier of SACs on MoS<sub>2</sub> could be calculated by Eq. (2) [40].

$$E_a = 0.636 \frac{E_{\text{binding}}^2}{E_c} - 0.203 \quad (2)$$

where E<sub>a</sub> is the diffusion barrier of SACs anchored on MoS<sub>2</sub>, E<sub>binding</sub> is the binding energy between a single metal atom and MoS<sub>2</sub>. Ec is the cohesive energy of the bulk metal.

For the formation energies of critical elementary steps, we used Eq. (3).

$$\Delta G_{*N_2H}^{\text{sol}} = G_{*N_2H}^{\text{sol}} - G_{*N_2}^{\text{sol}} - \frac{1}{2} G_{H_2}^{\text{sol}} \quad (3)$$

The formation energy of the PDS with implicit solvation correction was obtained by Eq. (3). The computational formulas of other steps are similar in terms of formation energy ( $E^{\text{sol}} = G^{\text{sol}}$  for SAC@MoS<sub>2</sub>).

We found that the VASP implicit solvation model does not work well for a simple two-dimension material, especially for sulfide and carbide (see Table S2). Thus we used the solvation effects of the same intermediates adsorbed on the Au surface, which we found to be approximately the same for Au (111), Au (110), or Au (100) (see Tables S3, S4). Thus we substituted the solvation effect of SAC@MoS<sub>2</sub> for various intermediates with the revised energies of the reaction intermediates of NRR on Au(100).

We take the Gibbs free energy of the proton-electron pair to be half of the energy of the H<sub>2</sub> molecule [41].

The correction in the free energy change from the applied electrode potential U is defined as:

$$\Delta G(U) = \Delta G(0) - neU \quad (4)$$

where neU is the change in the chemical potential of the proton-electron pair when the external potential U is applied [42].  $\Delta G_{\text{max}}$  is the formation energy of the PDS in NRR. For the highest barrier step, the onset potential (the limiting potential) is obtained through the equation  $U_{\text{limiting}} = -\Delta G_{\text{max}}/e$  ( $\Delta G_{\text{max}} = G_{\text{limiting}}$ ).

### 3 Results and Discussion

#### 3.1 The Mechanisms of NRR on Fe@MoS<sub>2</sub>

We first studied in detail the reaction mechanism of NRR on Fe@MoS<sub>2</sub>. Figure 1a is a schematic of the Fe@MoS<sub>2</sub>

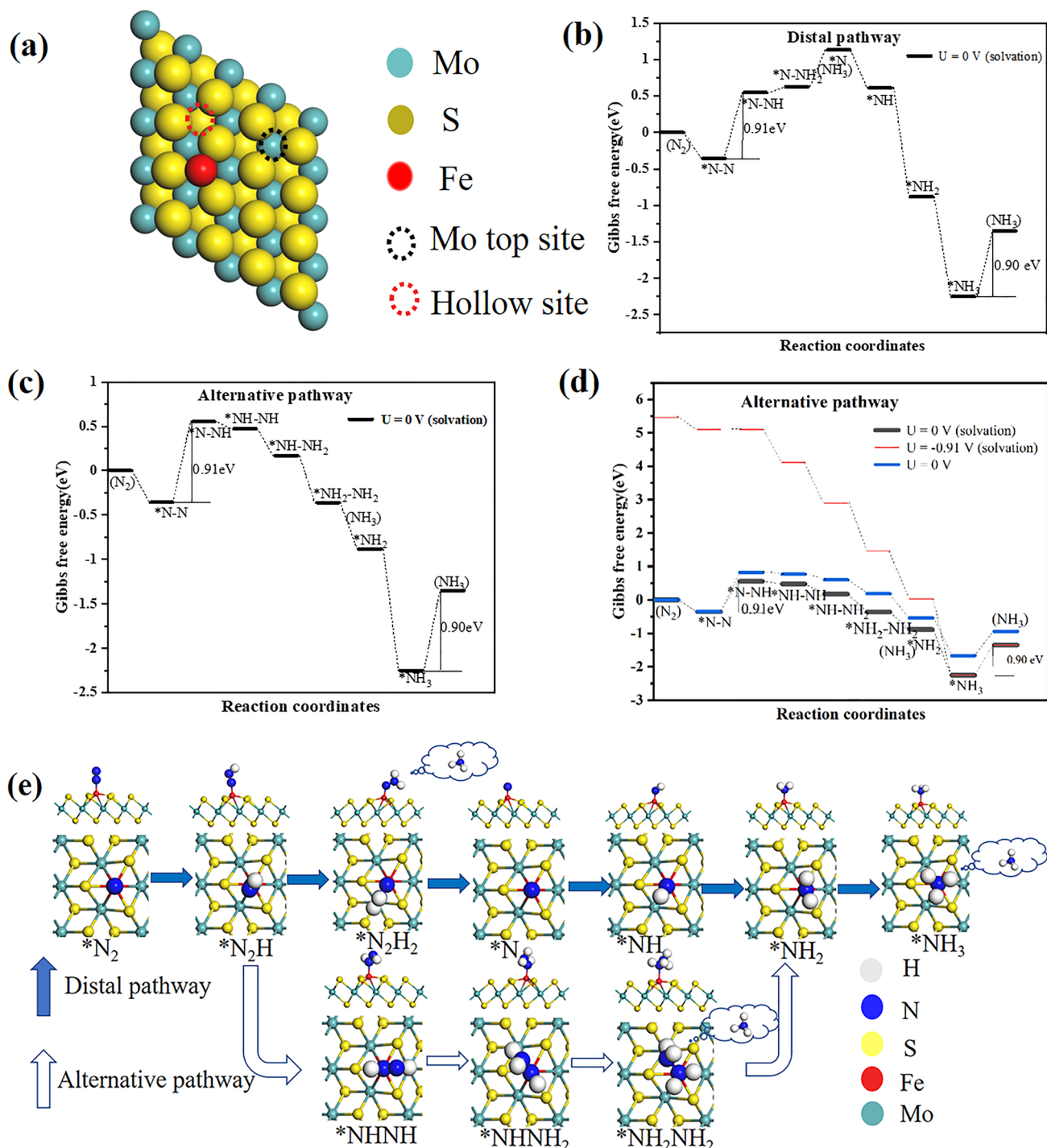


**Fig. 1** **a** A top view of a  $4 \times 4 \times 1$   $\text{MoS}_2$  supercell with Fe anchored on the hollow position. The colors are Mo in cyan, S in yellow, and Fe in red; The red and black circle denote the hollow and Mo top sites, respectively. **b** Distal pathway of NRR on  $\text{Fe}@\text{MoS}_2$ . **c** Alternative pathway of NRR on  $\text{Fe}@\text{MoS}_2$ ; **d** shows the alternative pathway

including implicit solvation for applied potential of 0 and  $0.91 \text{ V}_{\text{RHE}}$ ; **e** schematic for the two mechanisms for NRR on the  $\text{Fe}@\text{MoS}_2$ . These correspond with the reaction intermediates in the picture of **b** and **c**. The solid arrows indicate the Distal pathway; the blank arrows indicate the Alternative pathway

structure. There exist two active sites. One is the hollow site. The other is Mo top site. The distal pathway and alternative pathway on  $\text{Fe}@\text{MoS}_2$  are shown in Fig. 1b, c. The

comparison of these pathways is shown in Fig. 1d. Figure 1e depicts the intermediates on  $\text{Fe}@\text{MoS}_2$  for the two reaction pathways. Different from molybdenum complex

in which  $N_2$  vertically adsorbed on metal site [43, 44], only parallel adsorbed  $N_2$  can be reduced on  $Fe@MoS_2$ , while vertically adsorbed  $N_2$  is hardly be reduced (see Fig. S1). For the distal pathway in Fig. 1b, the absorption process of  $N_2$  is favorable (taking solvation effect into consideration) and is the same as one of the alternative pathways in Fig. 1c. This shows that  $N_2$  can be absorbed on the metal site instead of  $H_2O$ , but the first hydrogenation of  $N_2$  leads to a formation energy 0.91 eV higher. The formation energy is endothermic for various steps until the first N is formed, which is accompanied by release of one  $NH_3$ . Unfortunately, to desorb the final  $NH_3$  requires 0.90 eV, so that  $NH_3$  poisons the catalyst.

However, the alternative pathway in Fig. 1c has exothermic elementary steps after the first hydrogenation, except for  $NH_3$  desorption, making this alternative pathway better than the distal pathway for forming the first  $NH_3$  product, since the distal path needs a much higher onset potential. Figure 1d shows that the alternative pathway is favorable for an applied potential of 0.91 V<sub>SHE</sub>. The implicit solvation model corrects the Gibbs free energies of reaction intermediates, making NRR about 0.2 eV more favorable.

From the above results, we find

- the adsorption process of  $N_2$ ,
- the desorbed process of  $NH_3$ ,
- the PDS of the first hydrogenation of  $N_2$ , and
- the competitive reaction HER

all play important roles in the catalytic activity and selectivity of SAC@ $MoS_2$  on NRR.

### 3.2 The Structural Stabilities of SACs@ $MoS_2$

Structural stability is a prerequisite for high-performance electrocatalysis. We calculated the diffusion barrier and binding energy (details see in Fig S2, Tables S5 and S6) between SAC and  $MoS_2$  for both the Hollow site and Mo top site, the structures can be seen from Fig. 1a.

Calculating the DFT diffusion barrier for all 23 elements would require a great deal of computer time, but based on Eq. (2), we discovered that the formula from LASSO (Least absolute shrinkage and selection operator) regression (machine-learning method) is perfectly suited for our research system. The LASSO method can accurately describe the trend of the stability of SAC@ $MoS_2$ , saving computational costs. As shown in Fig. 2, Ti, Cr, Co, Ni, Zr, Nb, Ru, Rh, Ta, Re, Os, Ir, Pt have a diffusion barrier on  $MoS_2$  above 1.5 eV, which we consider is too high.

### 3.3 Electrochemical Catalytic Activity of SAC@ $MoS_2$ on NRR

To predict catalytic activity, we studied the three key steps.

First, for absorbed  $N_2$ , Fig. 3a shows that the absorption energies of  $N_2$  on SAC@ $MoS_2$  (hollow site) are always smaller than that on SAC@ $MoS_2$  (Mo top site). Thus we used the SACs@ $MoS_2$  (Mo top site) structures for subsequent calculations. Figure 3a shows that  $N_2$  can absorb on most SACs@ $MoS_2$ , with the highest absorption energy of ~1.20 eV for Re@ $MoS_2$  (Mo top site) and W@ $MoS_2$  (Mo top site). This first step of activating  $N_2$  shows a favorable start for NRR.

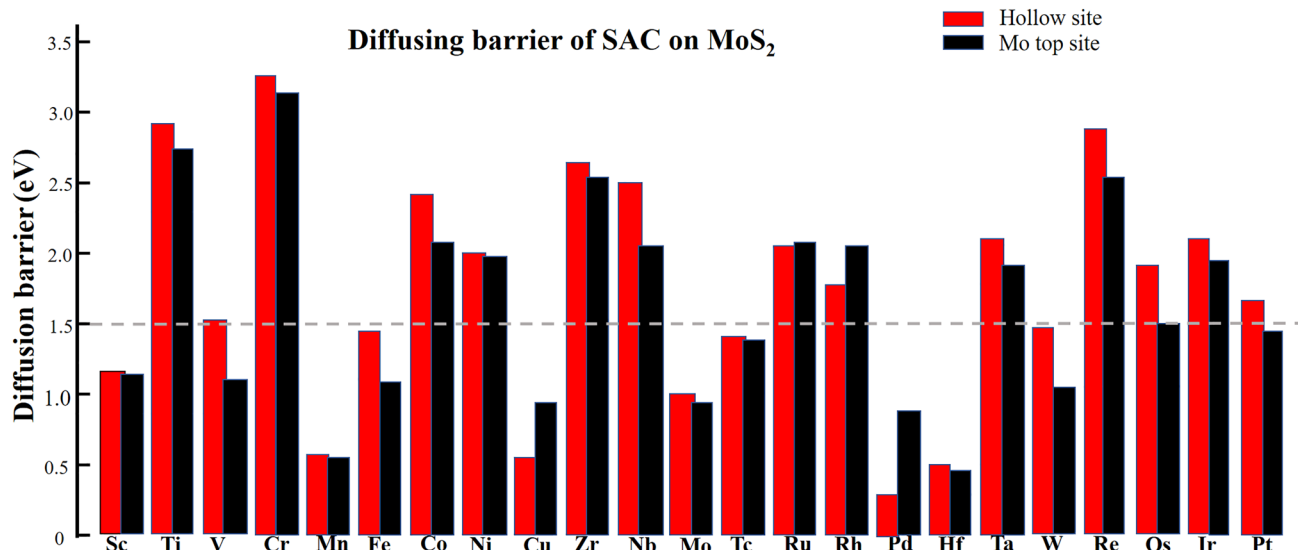


**Fig. 2** The diffusion barrier of single transition metal atom anchored on  $MoS_2$  (hollow site and Mo top site) including Sc, Ti, V, Cr, Mn, Fe, Co, Ni, Cu, Zr, Nb, Mo, Tc, Ru, Rh, Pd, Hf, Ta, W, Re, Os, Ir, Pt and the diffusion barrier above 1.5 eV is too high with a dotted line

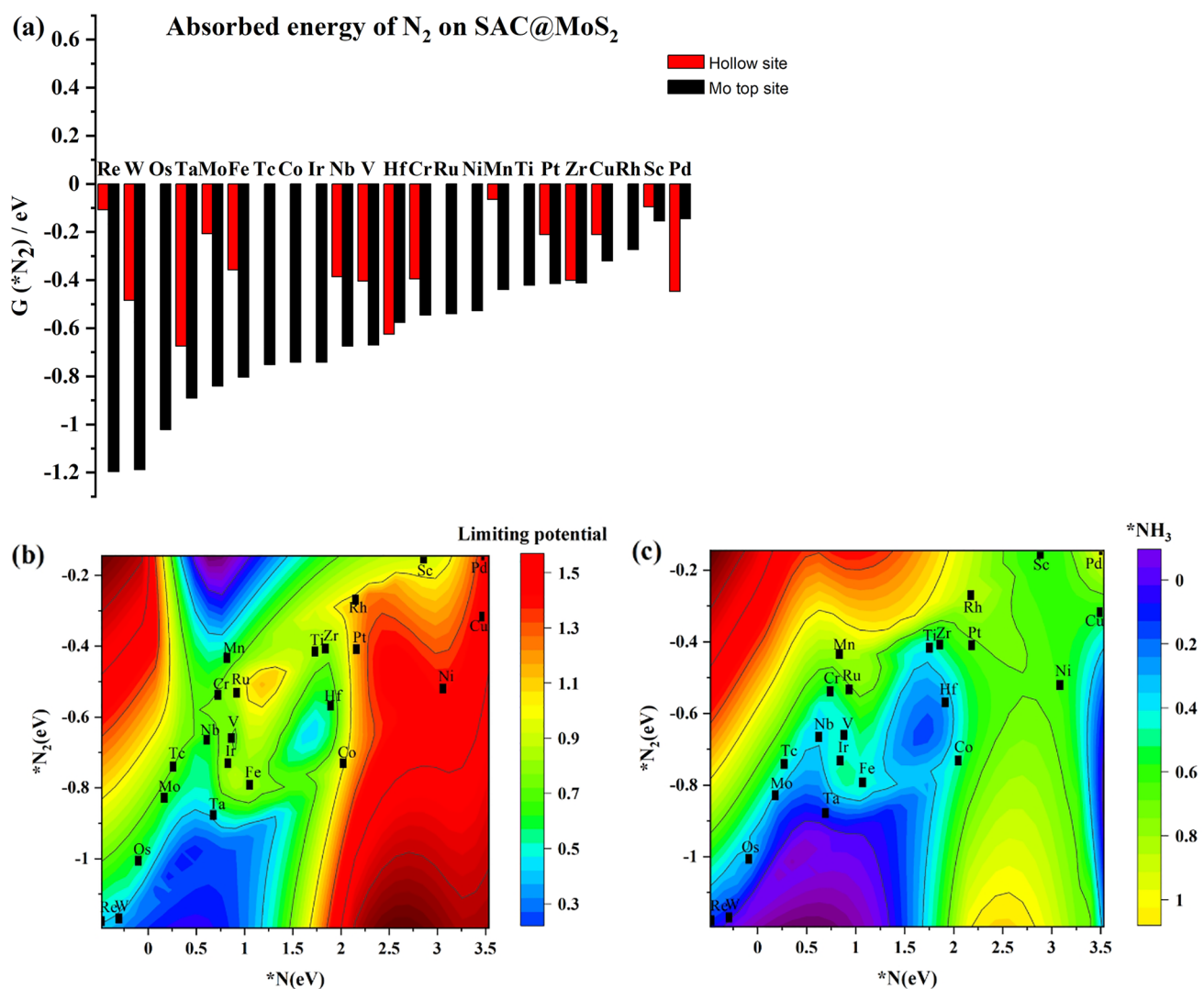


**Fig. 3** **a** The absorbed energies of N<sub>2</sub> on various SACs@MoS<sub>2</sub>, Os@MoS<sub>2</sub>, Tc@MoS<sub>2</sub>, Co@MoS<sub>2</sub>, Ir@MoS<sub>2</sub>, Ru@MoS<sub>2</sub>, Ni@MoS<sub>2</sub>, Ti@MoS<sub>2</sub> and Rh@MoS<sub>2</sub> (hollow site) are unfavorable for absorbed N<sub>2</sub>; **b** the distribution of the absorbed energies of N<sub>2</sub> and the limiting

potential with the absorbed energies of single atom N; **c** the distribution of the absorbed energies of N<sub>2</sub> and the desorbed energies of NH<sub>3</sub> with the absorbed energies of single atom N

Then, the first hydrogenation of N<sub>2</sub> and the desorption of NH<sub>3</sub> severely limit the NRR for SAC@MoS<sub>2</sub>. For further analysis, we chose the absorbed energy of single atom N as descriptors to describe the catalytic processes:

- (1) absorption energy of N<sub>2</sub>,
- (2) the limiting potential,
- (3) the desorption energy of NH<sub>3</sub>.

Figure 3b shows that Re@MoS<sub>2</sub>, W@MoS<sub>2</sub>, and Ta@MoS<sub>2</sub> are close to the blue area, with the lowest limiting potential for the Potential Determining Step (PDS) and the highest absorption energy for N<sub>2</sub>.

Figure 3c shows that Pd@MoS<sub>2</sub>, Rh@MoS<sub>2</sub>, and Mn@MoS<sub>2</sub> locate in the green area, with lower NH<sub>3</sub> desorption energies but weaker absorbed energy with N<sub>2</sub>.

Although no SAC@MoS<sub>2</sub> catalyst can satisfy all three factors, low limiting potential, low desorption energy of NH<sub>3</sub>, and high binding energy of N<sub>2</sub>, simultaneously, Ir@MoS<sub>2</sub>, Mn@MoS<sub>2</sub>, Ru@MoS<sub>2</sub>, Cr@MoS<sub>2</sub>, and Rh@MoS<sub>2</sub> stand for a balance shown as light green area in Fig. 3b, c, indicating a promising activity. Meanwhile, four of these cases have strong interaction with N<sub>2</sub> and good structural stabilities. Therefore, we paid special attention to these four candidates by further exploring their HER activity that help us to predict the Faraday efficiency (FE) of NRR.

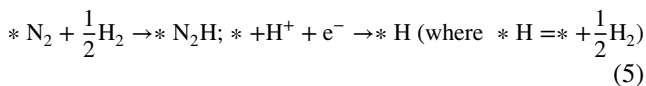
**Table 1**  $\Delta G(\text{HER})$  and  $\Delta G(\text{NRR})$  represent the Gibbs free energy change of PDS separately (FE Faraday efficiency)

Anchored atom	Mn	Ir	Sc	Tc	Cr	Nb	Mo	Hf	Os	Ti	Ta	Re
$\Delta G(\text{HER})/\text{eV}$	0.19	0.77	0.32	0.21	0.17	0.40	0.30	0.40	0.77	0.15	0.77	0.89
FE (%)	68.54	64.11	53.61	44.46	42.55	33.73	41.33	30.60	28.39	16.77	15.75	14.77
Anchored atom	V	W	Fe	Zr	Pt	Co	Ni	Cu	Ru	Rh	Pd	
$\Delta G(\text{HER})/\text{eV}$	0.06	0.91	0.11	0.07	0.43	0.18	0.34	0.22	0.02	0.27	0.51	
FE (%)	12.13	11.50	6.32	0.33	0.13	0	0	0	0	0	0	

An anchored atom represents a single atom anchored on Mo top site; others include major transition elements

### 3.4 Selectivity of SAC@MoS<sub>2</sub> Catalysts on NRR

In the mechanism for NRR on the SAC, the proton binds directly to \*N<sub>2</sub>. However, HER remains competitive. The Faraday efficiency (FE) is the generic standard to indicate which reaction is advantageous. As adopted in the work of Yang et al. [45], the PDS of NRR and HER are



Formulas (5) represent the PDS (Potential Determined Step) of NRR (Nitrogen Reduction Reaction) and HER (Hydrogen Evolution Reaction) separately.

$$\Delta G_1 = \Delta G_{\text{NH}_3} - \Delta G_{\text{NRR}} \quad (6)$$

$$\Delta G_2 = \Delta G_{\text{HER}} - \Delta G_{\text{NRR}} \quad (7)$$

$$FE = \frac{1}{1 + \exp\left(-\frac{\Delta G_2}{KT}\right)} \quad (8)$$

$$FE = \left(1 - \left(\frac{e^{\Delta G_1} - e^{-\Delta G_1}}{e^{\Delta G_1} + e^{-\Delta G_1}}\right)\right) \frac{1}{1 + \exp\left(-\frac{\Delta G_2}{KT}\right)} \quad (9)$$

In Eq. (6),  $\Delta G_{\text{NH}_3}$  represents the desorption energy of NH<sub>3</sub> on SAC@MoS<sub>2</sub>,  $\Delta G_{\text{NRR}}$  represents the formation energy of the first hydrogenation during NRR on SAC@MoS<sub>2</sub>,  $\Delta G_1$  represents the free energy difference of two elementary steps which is used for seeking a comprehensively balanced SAC@MoS<sub>2</sub> catalyst.

In Eq. (7),  $\Delta G_{\text{HER}}$  represents the formation energy of PDS on HER,  $\Delta G_{\text{NRR}}$  represents the formation energy of PDS on NRR,  $\Delta G_2$  equals the free energy difference of PDS between two competitive reactions, used for showing which is in advantage.

In Eq. (8), the selectivity of NRR is simply estimated according to Boltzmann distribution that is  $FE = 1 / (1 + \exp(-\Delta G_2/KT))$ . Where  $\Delta G_2$  is the free energy

difference between two competitive reactions at the same time, K is the Boltzmann constant, and T is temperature.

In Eq. (9), we introduce an amendment  $(1 - \left(\frac{e^{\Delta G_1} - e^{-\Delta G_1}}{e^{\Delta G_1} + e^{-\Delta G_1}}\right))$  in original Eq. (8) to compute FE for a more accurate prediction.

In addition, to adjust our calculated results to match the experiment, we include the value of FE (12.5%) on Fe@MoS<sub>2</sub> based on previous experiments [46, 47] to correct the limiting potential on HER (see Tables S7, S8) [39]. Using formulas (5), (6), and (8), leads to the calculated results shown in Table 1. We see that Ir@MoS<sub>2</sub> has a higher FE value with a higher structural stability, 64.11%, among SACs@MoS<sub>2</sub> on NRR. Therefore, we consider Ir@MoS<sub>2</sub> as the best candidate as the optimal catalyst on NRR.

## 4 Conclusion

Based on our reaction mechanism, the key reaction steps, and the FE for NRR, we consider Ir@MoS<sub>2</sub> to be the best catalyst candidate for NRR. Ir@MoS<sub>2</sub> has a relatively low onset potential limiting potential of 0.86 eV, higher selectivity of 64.11%, and lower desorption energy for NH<sub>3</sub> of 1.24 eV. The high diffusion barrier of 1.95 eV is also favorable, because it is beneficial to keep the single metal site from sintering. Therefore, Ir@MoS<sub>2</sub> with a high diffusion barrier is predicted to be stable to retain the high activity. Overall, we recommend Ir@MoS<sub>2</sub> (Mo top site) as the best electrochemical catalyst among SACs@MoS<sub>2</sub> on NRR. We hope these results provide guidance and directions for the experiments.

**Supplementary Information** The online version contains supplementary material available at <https://doi.org/10.1007/s11244-021-01546-6>.

**Acknowledgements** TC thanks to the National Natural Science Foundation of China (21903058), the Natural Science Foundation of Jiangsu Higher Education Institutions (SBK20190810), the Jiangsu Province High-Level Talents (JNHB-106), the Priority Academic Program Development of Jiangsu Higher Education Institutions (PAPD) for financial support. HY thanks China Postdoctoral Science Foundation (2019M660128) for financial support. This work was partly supported

by the Collaborative Innovation Center of Suzhou Nano Science & Technology. WAG thanks NSF (CBET-2005250) for support.

## Declarations

**Conflict of interest** The authors declare no conflict of interest.

## References

- Foster SL, Bakovic SIP, Duda RD, Maheshwari S, Milton RD, Minteer SD, Janik MJ, Renner JN, Greenlee LF (2018) *Nat Catal* 1:490–500
- Erisman JW, Sutton MA, Galloway J, Klimont Z, Winiwarter W (2008) *Nat Geosci* 1:636–639
- Su H, Chen L, Chen Y, Si R, Wu Y, Wu X, Geng Z, Zhang W, Zeng J (2020) *Angew Chem Int Ed Engl* 59:20411–20416
- Capdevila-Cortada M (2019) Electrifying the Haber-Bosch. *Nat Catal* 2:1055
- Suryanto BHR, Du H-L, Wang D, Chen J, Simonov AN, MacFarlane DR (2019) *Nat Catal* 2:290–296
- Zhang L, Ji X, Ren X, Ma Y, Shi X, Tian Z, Asiri AM, Chen L, Tang B, Sun X (2018) *Adv Mater* 30:1800191
- Chen LY, Kuo TC, Hong ZS, Cheng MJ, Goddard WA (2019) *Phys Chem Chem Phys* 21:17605–17612
- Bao D, Zhang Q, Meng F-L, Zhong H-X, Shi M-M, Zhang Y, Yan J-M, Jiang Q, Zhang X-B (2017) *Adv Mater* 29:1604799
- Yang D, Chen T, Wang Z (2017) *J Mater Chem A* 5:18967–18971
- Logadóttir Á, Nørskov JK (2003) *J Catal* 220:273–279
- Xue Z-H, Zhang S-N, Lin Y-X, Su H, Zhai G-Y, Han J-T, Yu Q-Y, Li X-H, Antonietti M, Chen J-S (2019) *J Am Chem Soc* 141:14976–14980
- Das A, Nair AS, Pathak B (2020) *J Phys Chem C* 124:20193–20202
- Ma X, Hu J, Zheng M, Li D, Lv H, He H, Huang C (2019) *Appl Surf Sci* 489:684–692
- Abghouli Y, Garden AL, Hlynsson VF, Björgvinsdóttir S, Ólafsdóttir H, Skúlason E (2015) *Phys Chem Chem Phys* 17:4909–4918
- Abghouli Y, Skúlason E (2017) *J Phys Chem C* 121:24036–24045
- Ramaiyan KP, Ozden S, Maurya S, Kelly D, Babu SK, Benavidez A, Garzon FG, Kim YS, Kreller CR, Mukundan R (2020) *J Electrochem Soc* 167:044506
- Huang L, Wu J, Han P, Al-Enizi AM, Almutairi TM, Zhang L, Zheng G (2019) *Small Methods* 3:1800386
- Xiang X, Wang Z, Shi X, Fan M, Sun X (2018) *ChemCatChem* 10:4530–4535
- Ye TN, Park SW, Lu Y, Li J, Sasase M, Kitano M, Tada T, Hosono H (2020) *Nature* 583:391–395
- Lü F, Zhao S, Guo R, He J, Peng X, Bao H, Fu J, Han L, Qi G, Luo J, Tang X, Liu X (2019) *Nano Energy* 61:420–427
- Yang Y, Zhang L, Hu Z, Zheng Y, Tang C, Chen P, Wang R, Qiu K, Mao J, Ling T, Qiao SZ (2020) *Angew Chem Int Ed Engl* 59:4525–4531
- Yang T, Song TT, Zhou J, Wang S, Chi D, Shen L, Yang M, Feng YP (2020) *Nano Energy* 68:104304
- Howard JB, Rees DC (1996) *Chem Rev* 96:2965–2982
- Ling F, Liu X, Jing H, Chen Y, Zeng W, Zhang Y, Kang W, Liu J, Fang L, Zhou M (2018) *Phys Chem Chem Phys* 20:26083–26090
- Zhang J, Zhang H, Wu T, Wang Q, van der Spoel D (2017) *J Chem Theory Comput* 13:1034–1043
- Kresse G, Hafner J (1993) *Phys Rev B* 48:13115–13118
- Kresse G, Hafner J (1993) *Phys Rev B* 47:558–561
- Kresse G, Joubert D (1999) *Phys Rev B* 59:1758–1775
- Perdew JP, Burke K, Ernzerhof M (1996) *Phys Rev Lett* 77:3865–3868
- Perdew JP, Wang Y (1992) *Phys Rev B* 45:13244–13249
- Grimme S, Antony J, Ehrlich S, Krieg H (2010) *J Chem Phys* 132:154104
- Grimme S, Ehrlich S, Goerigk L (2011) *J Comput Chem* 32:1456–1465
- Makov G, Payne MC (1995) *Phys Rev B* 51:4014–4022
- Neugebauer J, Scheffler M (1992) *Phys Rev B* 46:16067–16080
- Mathew K, Kolluru VSC, Mula S, Steinmann SN, Hennig RG (2019) *J Chem Phys* 151:234101
- Qian J, An Q, Fortunelli A, Nielsen RJ, Goddard WA III (2018) *J Am Chem Soc* 140:6288–6297
- An Q, Shen Y, Fortunelli A, Goddard WA III (2018) *J Am Chem Soc* 140:17702–17710
- Singh AR, Rohr BA, Statt MJ, Schwalbe JA, Cargnello M, Nørskov JK (2019) *ACS Catal* 9:8316–8324
- Bjork J (2016) *J Phys Chem C* 120:21716–21721
- Su Y-Q, Zhang L, Wang Y, Liu J-X, Muravev V, Alexopoulos K, Filot IAW, Vlachos DG, Hensen EJM (2020) *npj Comput Mater* 6:144. <https://doi.org/10.1038/s41524-020-00411-6>
- Norskov JK, Rossmeisl J, Logadóttir A, Lindqvist L, Kitchin JR, Bligaard T, Jonsson H (2004) *J Phys Chem B* 108:17886–17892
- Skulason E, Bligaard T, Gudmundsdóttir S, Studt F, Rossmeisl J, Abild-Pedersen F, Vegge T, Jonsson H, Norskov JK (2012) *Phys Chem Chem Phys* 14:1235–1245
- Arashiba K, Miyake Y, Nishibayashi Y (2011) *Nat Chem* 3:120–125
- Arashiba K, Kinoshita E, Kuriyama S, Eizawa A, Nakajima K, Tanaka H, Yoshizawa K, Nishibayashi Y (2015) *J Am Chem Soc* 137:5666–5669
- Zhao W, Zhang L, Luo Q, Hu Z, Zhang W, Smith S, Yang J (2019) *ACS Catal* 9:3419–3425
- Guo J, Tadesse Tsega T, Ul Islam I, Iqbal A, Zai J, Qian X (2020) *Chin Chem Lett* 2020(31):2487–2490
- Guo J, Wang M, Xu L, Li X, Iqbal A, Sterbinsky GE, Yang H, Xie M, Zai J, Feng Z, Cheng T, Qian X (2021) *Chin J Chem* 39:1898–1904

**Publisher's Note** Springer Nature remains neutral with regard to jurisdictional claims in published maps and institutional affiliations.